Bioactive Materials 35 (2024) 135–149

Contents lists available at ScienceDirect

Bioactive Materials

journal homepage: www.keaipublishing.com/en/journals/bioactive-materials

Extracellular vesicles released by transforming growth factor-beta 1-preconditional mesenchymal stem cells promote recovery in mice with spinal cord injury

Guoliang Chen [a,b,c,1], Shiming Li [c,1], Kuileung Tong [c,1], Zerong Huang [a,1], Shuangjiang Liu [a,b], Haoran Zhu [d], Yanheng Zhong [a], Zhisen Zhou [b,*], Genlong Jiao [b,a,**], Fuxin Wei [c,***], Ningning Chen [c,****]

[a] Department of Orthopedic Surgery, The First Affiliated Hospital of Jinan University, Guangzhou, 510632, China
[b] Dongguan Key Laboratory of Central Nervous System Injury and Repair / Department of Orthopedic Surgery, The Sixth Affiliated Hospital of Jinan University (Dongguan Eastern Central Hospital), Dongguan, 523573, China
[c] Department of Orthopedic Surgery, The Seventh Affiliated Hospital, Sun Yat-sen University, Shenzhen, 518107, China
[d] Department of Orthopedic Surgery, The Fifth Affiliated Hospital of Jinan University (Heyuan Shenhe People's Hospital), Heyuan, 517400, China

ARTICLE INFO

Keywords:
Endogenous neural stem cells
Extracellular vesicles
Mesenchymal stem cells
mTORC2/rictor pathway
Spinal cord injury
TGF-β1

ABSTRACT

Spinal cord injury (SCI) causes neuroinflammation, neuronal death, and severe axonal connections. Alleviating neuroinflammation, protecting residual cells and promoting neuronal regeneration via endogenous neural stem cells (eNSCs) represent potential strategies for SCI treatment. Extracellular vesicles (EVs) released by mesenchymal stem cells have emerged as pathological mediators and alternatives to cell-based therapies following SCI. In the present study, EVs isolated from untreated (control, C-EVs) and TGF-β1-treated (T-EVs) mesenchymal stem cells were injected into SCI mice to compare the therapeutic effects and explore the underlying mechanisms. Our study demonstrated for the first time that the application of T-EVs markedly enhanced the proliferation and antiapoptotic ability of NSCs *in vitro*. The infusion of T-EVs into SCI mice increased the shift from the M1 to M2 polarization of reactive microglia, alleviated neuroinflammation, and enhanced the neuroprotection of residual cells during the acute phase. Moreover, T-EVs increased the number of eNSCs around the epicenter. Consequently, T-EVs further promoted neurite outgrowth, increased axonal regrowth and remyelination, and facilitated locomotor recovery in the chronic stage. Furthermore, the use of T-EVs in *Rictor*$^{-/-}$ SCI mice (conditional knockout of *Rictor* in NSCs) showed that T-EVs failed to increase the activation of eNSCs and improve neurogenesis sufficiently, which suggested that T-EVs might induce the activation of eNSCs by targeting the mTORC2/Rictor pathway. Taken together, our findings indicate the prominent role of T-EVs in the treatment of SCI, and the therapeutic efficacy of T-EVs for SCI treatment might be optimized by enhancing the activation of eNSCs via the mTORC2/Rictor signaling pathway.

1. Introduction

Traumatic spinal cord injury (SCI) is an irreversible disease that leads to persistent sensory and motor deficits below the level of injury [1,2]. The pathophysiology of SCI is complex and includes both primary injury and secondary injury [3,4]. Primary injury mechanically damages neural cells and the blood–spinal cord barrier directly, and secondary injury is subsequently induced by prolonged immune responses and

Peer review under responsibility of KeAi Communications Co., Ltd.
* Corresponding author.
** Corresponding author. Dongguan Key Laboratory of Central Nervous System Injury and Repair / Department of Orthopedic Surgery, The Sixth Affiliated Hospital of Jinan University (Dongguan Eastern Central Hospital), Dongguan, 523573, China.
*** Corresponding authors. Department of Orthopedic Surgery, The Seventh Affiliated Hospital, Sun Yat-sen University, China.
**** Corresponding author. Department of Orthopedic Surgery, The Seventh Affiliated Hospital, Sun Yat-sen University, China.
E-mail addresses: zhouzs1009@163.com (Z. Zhou), tjglong@jnu.edu.cn (G. Jiao), weifuxin@mail.sysu.edu.cn (F. Wei), chennn8@mail.sysu.edu.cn (N. Chen).
[1] These authors contributed equally to this study.

https://doi.org/10.1016/j.bioactmat.2024.01.013
Received 12 December 2023; Received in revised form 10 January 2024; Accepted 15 January 2024

neuroinflammation [5]. Secondary injury not only worsens the extent of SCI but also inhibits neural regeneration due to the undesirable post-injury microenvironment [6]. In regeneration-competent species such as teleost fish, urodeles and some lizards, endogenous neural stem cells (eNSCs) are rapidly recruited to the lesion site, where they give rise to differentiated cells and integrate into the newly formed tissue [7,8]. Like in regeneration-competent species, in response to SCI in mammals, eNSCs in the periventricular zone surrounding the central canal within the spinal cord can be activated after injury and proliferate, migrate to the site of injury, and differentiate into mature neural cells [9]. However, accumulating studies related to mammals have demonstrated that the activation of eNSCs is insufficient for structural repair or functional recovery following SCI [10–12]. Moreover, activated eNSCs exhibit limited migration to neighboring injury sites and usually differentiate into astrocytes owing to pathological conditions [13,14]. Enhancing and modulating the proliferation, migration, and neuronal differentiation of eNSCs may improve neurological outcomes in patients with SCI [15].

Stem cell-based therapy is regarded as a promising strategy for treating SCI due to the immunomodulation and trophic support of stem cells [16]. Among stem cells, mesenchymal stem cells (MSCs) are particularly attractive for SCI repair because of their relative ease of access and efficient *in vitro* expansion [17]. Several studies have revealed that umbilical cord MSCs can be easily obtained without ethical issues, and in addition, umbilical cord MSCs have been shown to have superior differentiation, migration, and protection properties compared with other types of stem cells [18,19]. The transplantation of MSCs can reduce the injury volume and further promote neuronal and axonal regeneration [20], but the application of these cells is limited by their tumorigenicity, low survival rate, and immune rejection [21]. Emerging evidence has revealed that the efficacy of MSC treatment for SCI results mainly from paracrine effects instead of from the transdifferentiation and implantation of MSCs [22,23]. Alternatively, extracellular vesicles (EVs), which are released into the extracellular environment by almost all types of cells, exist widely in body fluids and mainly participate in the paracrine signaling of cells; these vesicles are attracting increased amounts of research attention [24]. EVs from MSCs were confirmed to facilitate functional recovery after SCI via various mechanisms, including anti-inflammatory effects, regulation of macrophage polarization and protection of the blood–spinal cord barrier in SCI [23,25]. It is still unclear whether MSC-derived EVs play a role in the activation of eNSCs following SCI. Importantly, EVs from different preconditioned MSCs (such as hypoxic [26] or drug-treated [27] MSCs) are suggested to have different effects. Transforming growth factor-beta 1 (TGF-β1), a widely used growth factor, was demonstrated to modulate multiple cellular functions during development and tissue homeostasis. Furthermore, TGF-β1 was confirmed to boost the proliferation and functionality of MSCs [28]; additionally, TGF-β1 was demonstrated to play a protective role against microglia-mediated neuroinflammation in an *in vitro* stroke model [29]. EV generation is associated with the proliferation rate of MSCs [30]. However, whether TGF-β1 can be utilized to alter MSC-derived EV production and enhance the efficacy of EVs for the treatment of SCI has not been determined. We speculated that TGF-β1 can facilitate the release and modification of the components of MSC-derived EVs, which may improve their therapeutic efficacy in treating SCI.

In the present study, EVs derived from untreated (control, C-EVs) or TGF-β1-pretreated (T-EVs) umbilical cord MSCs were intravenously injected into SCI mice to compare therapeutic efficacy. Our results demonstrated stronger recovery in T-EV-treated SCI mice. In addition to reducing inflammation and improving the survival of residual cells, T-EVs exhibit an enhanced ability to regulate the proliferation and migration of eNSCs in the acute phase of SCI. Previous studies have shown the vital roles of the mTORC2/Rictor pathway in cell survival, proliferation, migration and cytoskeletal rearrangement [31]. A protein interaction network analysis of TGF-β1 was conducted using the STRING database, revealing a documented relationship with mTORC2 through both text mining and experimental determination (Supplementary file, Fig. S1). Our prior investigations focused on the function of the mTORC2/Rictor signaling pathway in the neuronal differentiation of transplanted NSCs for the treatment of SCI [32]. In this study, we sought to explore whether EVs secreted by TGF-β1-treated MSCs influence mTORC2/Rictor. Rictor is the core member of mTORC2; therefore, T-EVs were further injected into SCI mice with *Rictor* conditional knockout (*Rictor*$^{-/-}$) in NSCs (Nestin^{+}) to explore the relationships between T-EVs and the mTORC2/Rictor pathway and between T-EVs and the activation of eNSCs following SCI. Our results suggested that T-EVs might improve therapeutic efficacy by enhancing the activation of eNSCs via the mTORC2/Rictor pathway (Graphical abstract).

2. Results

2.1. TGF-β1 promotes the secretion of MSC-derived EVs

Three-line differentiation (Alizarin Red, Oil Red and Alcian Blue staining) was induced successfully in human umbilical cord MSCs (Supplementary file, Fig. S2A). Flow cytometry-based immunophenotyping of human umbilical cord MSCs further confirmed the negative expression (<2 %) of CD19, CD34, CD45, and HLA-DR and highly positive expression of CD73, CD90, and CD105 (>99 %) in human umbilical cord MSCs (Supplementary file, Fig. S2B).

EV generation is associated with the proliferation rate of MSCs [30], and EVs are generated from multivesicular bodies. CD63 is concentrated on multivesicular bodies and is considered the primary precursor of EVs [33]. To investigate the effects of TGF-β1 on the secretion of EVs by MSCs, we performed EdU staining to evaluate the proliferation rate of MSCs, and IF and Western blotting were also conducted to assess the expression of CD63 on MSCs. EdU staining revealed that the TGF-β1-treated MSCs had a significantly greater proliferation rate than the control MSCs (Supplementary file, Figs. S3A and C). Additionally, IF revealed that TGF-β1-treated MSCs had more intense CD63 staining than did control MSCs (Figs. S3B and D), while Western blot analysis also demonstrated increased expression of CD63 and Alix on TGF-β1-treated MSCs (Figs. S3E–F).

Furthermore, the size and morphology of the MSC-derived EVs were evaluated via TEM and nanoflow cytometry, and specific EV markers were examined via Western blotting. TEM (Fig. 1A) and nanoflow cytometry (Fig. 1B) revealed that the application of TGF-β1 did not affect the size or morphology of the EVs. Nanoflow cytometry-based EV concentration data demonstrated that the concentration of T-EVs was significantly greater (Fig. 1B–C). Moreover, Western blotting demonstrated that both CD63 and Alix protein levels were greater in TGF-β1-treated MSC-released EVs than in control MSCs. Importantly, calnexin, an endoplasmic reticulum marker, was negatively expressed in both groups, which indicated that the isolated EVs were not contaminated with other cell membranes (Fig. 1D). These results suggest that TGF-β1 may facilitate the secretion of EVs. To investigate whether the EVs arrived at the SCI center sufficiently, an *in vivo* imaging system (IVIS) was used to track the EVs after infusion via the tail vein. The results revealed that both C-EVs and T-EVs can reach the SCI site, while T-EVs might reach higher concentrations (Fig. 1E).

2.2. T-EVs enhance the proliferation, antiapoptotic and neuronal differentiation of NSCs in vitro

Genotyping of the mice was performed by PCR analysis of genomic DNA, which confirmed the successful generation of Nestin-*Rictor*$^{-/-}$ mice (Supplementary file, Figs. S4A–C). The NSC-specific *Rictor*-knockout mice showed no abnormalities in spinal cord morphology or function. For both wild-type (WT) and *Rictor*$^{-/-}$ mice, Nestin^{+} NSCs were located around the central canal of the spinal cord. Rictor was expressed in all cell types of the WT mice but was absent in the Nestin^{+} cells of the *Rictor*$^{-/-}$ mice (Supplementary file, Fig. S4D). NSCs isolated

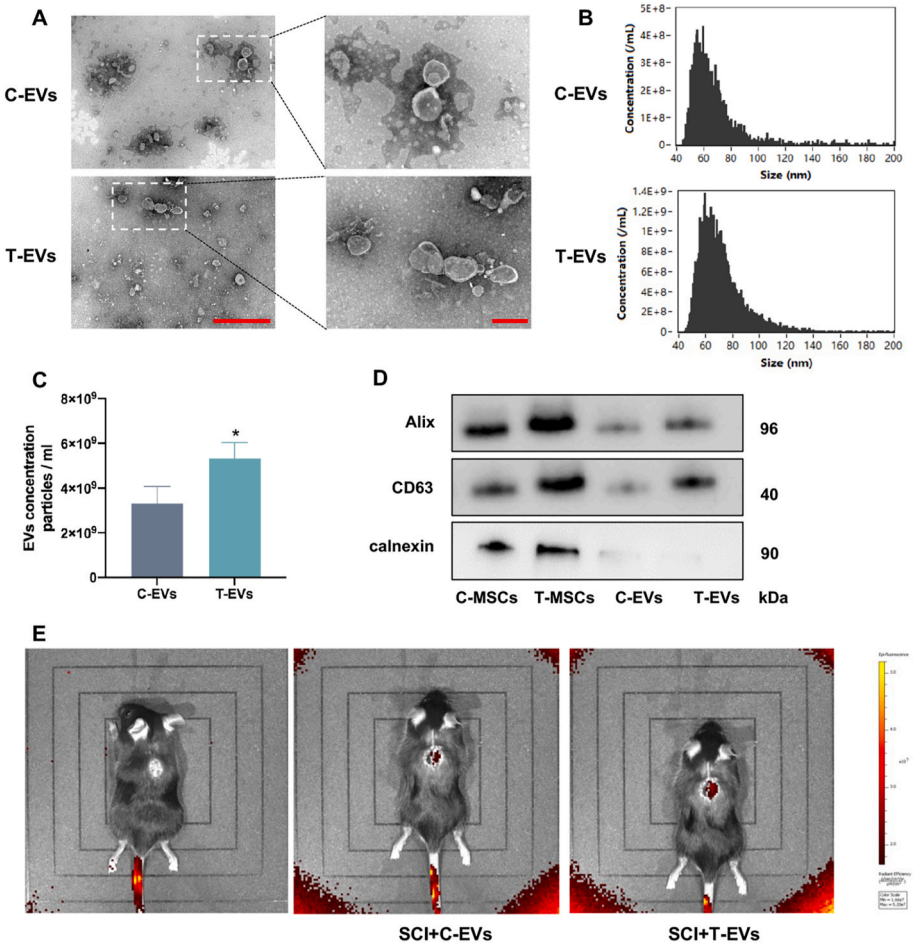

Fig. 1. TGF-β1 promotes the secretion of MSC-derived EVs
(A) TEM image of EVs isolated from C-MSCs and T-MSCs; low magnification: scale bar = 1 μm; high magnification: scale bar = 200 nm. (B) Nanoflow cytometry analysis of EVs from C-MSCs and T-MSCs. (C) Comparison of nanoflow cytometry analysis-based particle concentrations of C-EVs and T-EVs. (D) Western blotting analysis of the proteins Alix, CD63 and calnexin in C-MSCs, T-MSCs, C-EVs and T-EVs. (E) EV distribution in SCI mice based on an *in vivo* imaging system. $^{*}P < 0.05$.

from both WT and *Rictor*$^{-/-}$ mice were found to gather as neurospheres and abundantly express Nestin *in vitro* (Supplementary file, Fig. S4E), which confirmed that the cells used in this study were NSCs and that the CKO of *Rictor* did not influence the development of NSCs [32].

Furthermore, the effect of T-EVs on the proliferation of NSCs was evaluated via an EdU cell proliferation kit. As shown in the Supplementary file and Figs. S5A–B, the application of EVs not only increased the number of cells (increased confluence) but also overwhelmingly increased the proportion of EdU-positive cells. T-EVs had stronger effects on the proliferation of NSCs than C-EVs. Previous studies confirmed the vital role of the mTORC2/Rictor pathway in regulating cytoskeletal rearrangements and the survival and proliferation of cells. Western blotting demonstrated that the mTORC2/Rictor pathway was upregulated in EV-treated NSCs, especially in T-EV-treated NSCs (Supplementary file, Figs. S5C–D). Among *Rictor*$^{-/-}$ NSCs, the percentage of EdU-positive cells decreased. The application of T-EVs increased the proportion of EdU-positive cells among *Rictor*$^{-/-}$ NSCs, but T-EVs increased the proportion of EdU-positive cells among WT NSCs more strongly (Supplementary file, Figs. S5E–F). Western blot analysis of both WT and *Rictor*$^{-/-}$ NSCs revealed that T-EVs increased the expression of mTOR and P-mTOR, but the proliferation of *Rictor*$^{-/-}$ NSCs was inferior to that of WT NSCs (Supplementary file, Figs. S5G–H). These results suggest that T-EVs enhance the proliferation of NSCs via the mTORC2/Rictor pathway and that other pathways might be involved.

Previous studies revealed that NSCs also secrete growth factors to mediate the function of other cells after SCI. In the present study, the mRNA levels of growth factors, including EGF, BDNF and FGF, were evaluated via RT−PCR. As shown in the Supplementary file and Fig. S6A, EVs increased the relative mRNA levels of those growth factors, and T-EV-treated NSCs had higher mRNA levels of EGF, BDNF and FGF than did C-EV-treated NSCs. For *Rictor*$^{-/-}$ NSCs, the mRNA levels of those growth factors were significantly decreased (Supplementary file, Fig. S6B). Collectively, these results suggested that the application of T-EVs could enhance the stem cell function of NSCs by upregulating the mTORC2/Rictor pathway.

After treatment with EVs, NSCs were treated with TNF-α. Terminal deoxynucleotidyl transferase-mediated dUTP nick-end labeling (TUNEL) staining revealed that the number of TUNEL-positive cells was significantly lower in TNF-α+C-EV- and TNF-α+T-EV-treated NSCs than in TNF-α-treated NSCs. The proportion of TUNEL-positive cells among the TNF-α+C-EV-treated NSCs was between that among the TNF-α+T-EV-treated NSCs and that among the TNF-α-treated NSCs (Supplementary file, Figs. S7A–B). Similar and opposite expression levels of cleaved caspase-3 and Bcl-2, respectively, were detected via Western blotting (Supplementary file, Figs. S7C–D).

Fourteen days after the induction of differentiation, compared with those of the control NSCs, the proportions of MAP2-positive cells among the C-EV- and T-EV-treated NSCs increased significantly, whereas the numbers of MAP2-positive cells among the T-EV-treated NSCs were significantly greater than those among the C-EV-treated NSCs. In contrast, compared with those of the control NSCs, the number of cells with positive GFAP expression was significantly lower for both the C-EV-

and T-EV-treated NSCs, especially for the T-EV-treated NSCs (Supplementary file, Figs. S8A–B). Similar MAP2 and GFAP expression levels were detected via Western blotting (Supplementary file, Figs. S8C–D).

2.3. T-EVs increase the polarization of reactive microglia from the M1 to the M2 phenotype and alleviate neuroinflammation in vivo

Microglia are among the main resident cell types in the spinal cord, and reactive microglia are critical for the development and regulation of neuroinflammation after SCI. To determine the effects of T-EVs on the polarization of reactive microglia in SCI, macrophage phenotypes were assessed on the 7th day after SCI. Iba-1 is a typical microglial marker, and iNOS and Arginase-1 were used to distinguish the M1 and M2 subpopulations, respectively. Immunofluorescence staining of spinal cord sections from SCI + C-EVs and SCI + T-EVs significantly decreased the percentage of iNOS- and CD63-positive M1 macrophages and increased the proportion of Arginase-1 (Arg-1)-expressing M2 macrophages among the Iba-1-positive cells compared with those in the SCI group, and mice treated with T-EVs had fewer M1 macrophages and more M2 macrophages in the lesion site than did the C-EV-treated SCI mice (Fig. 2A–D, Supplementary file, Fig. S9). Furthermore, the expression levels of iNOS and Arg-1 at the lesion site were assessed via Western blotting on day 7 postinjury. Like those of immunofluorescence staining, the Western blot results also revealed differences in the

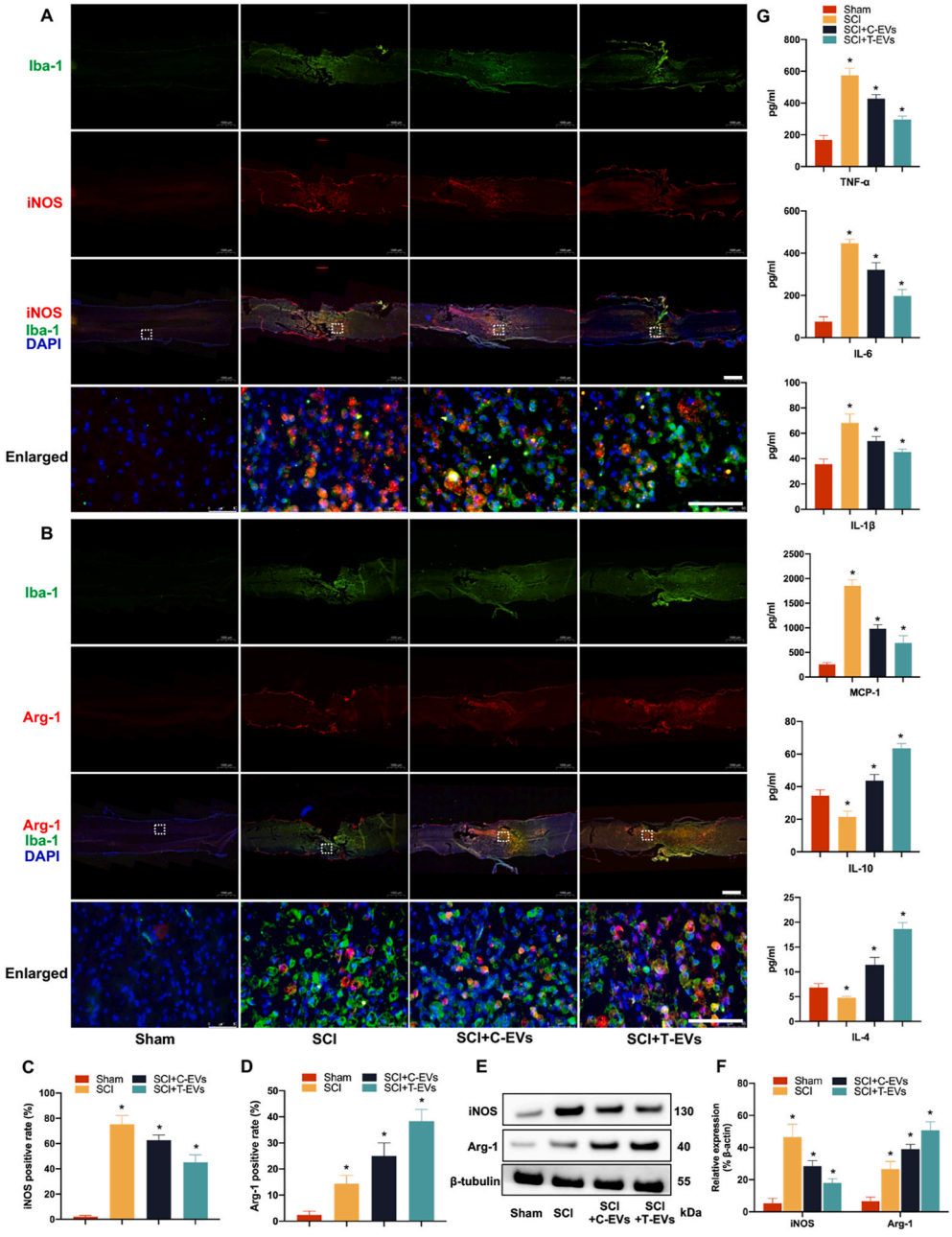

Fig. 2. T-EVs increase the polarization of reactive microglia from the M1 to the M2 phenotype and alleviate neuroinflammation *in vivo*
(A) Double immunofluorescence staining of M1 macrophages in the injured spinal cord; low magnification: scale bar = 1000 μm; high magnification: scale bar = 50 μm. (B) Double immunofluorescence staining of M1 macrophages in the injured spinal cord; low magnification: scale bar = 1000 μm; high magnification: scale bar = 50 μm. (C–D) Quantification of the relative percentage of M1 or M2 macrophages among the different groups. (E) Western blotting analysis of iNOS, Arg-1, and β-actin expression in the injured spinal cords of the various groups. (F) Quantification of the protein expression of iNOS and Arg-1 in the different groups. (G) The expression of inflammation-related cytokines in the spinal cords of the different groups was analyzed via ELISA. *$P < 0.05$.

expression of iNOS and Arg-1 among the SCI, SCI + C-EV and SCI + T-EV groups (Fig. 2E–F). Importantly, the severity of the inflammatory reaction was assessed by determining the concentrations of inflammatory mediators in the epicenter of SCI using an enzyme-linked immunosorbent assay (ELISA) on day 7 postinjury. As expected, samples from the SCI + T-EV group exhibited significantly lower expression of proinflammatory cytokines, including TNF-α, IL-6, IL-1β and MCP-1, and greater expression of anti-inflammatory cytokines, such as IL-10 and IL-4, than did those from the other injury groups (Fig. 2G). In summary, these results suggested that T-EVs promoted M2 macrophage polarization in the injured spinal cord and alleviated neuroinflammation by regulating the secretion of inflammation-related cytokines.

2.4. T-EVs improve neuroprotection in mice subjected to SCI

In addition to the primary injury caused by mechanical violence, neuroinflammation following SCI is considered a secondary injury that might lead to a long-term harmful effect on residual neural cells. The infusion of T-EVs was confirmed to play a positive role in alleviating neuroinflammation, and we further studied the neuroprotective function of T-EVs by evaluating the status of cells around the lesion center.

On day 7 postinjury, pronounced cell apoptosis, as indicated by TUNEL staining (Fig. 3A–C) and cleaved caspase-3 (Supplementary file, Figs. S10A and C) staining, was observed at the SCI site. Compared with the control treatment, the application of EVs significantly mitigated cellular apoptosis. T-EVs had the strongest ability to alleviate cell apoptosis, followed by C-EVs. Western blot analysis revealed a consistent expression pattern of cleaved caspase-3 compared to that observed through immunofluorescence staining, while Bcl-2 exhibited an inverse expression profile to cleaved caspase-3 (Fig. 3E–F).

Moreover, neurons located 5 mm rostral and caudal to the epicenter were utilized to investigate the neuroprotective effect of EVs on the remaining neuronal population. Transverse sections of the spinal cord were utilized for neuronal quantification via Nissl and NeuN staining techniques. The large size and increased number of Nissl bodies indicated that neural cells strongly function in protein synthesis, and NeuN is a marker of mature neurons. The number of cells stained positively was quantified and averaged per section in a blinded manner. The cells with positive Nissl staining (Fig. 3B–D) and NeuN staining (Supplementary file, Figs. S10B–C) were the most abundant in the sham group, followed by the SCI + T-EV$_S$, SCI + C-EVs, and control groups. These findings suggest that the administration of EVs following SCI can mitigate cellular apoptosis and augment the viability of neighboring neurons.

2.5. T-EVs increase the number of eNSCs around the epicenter in mice with SCI

After SCI, eNSCs expressing Nestin are activated in spared neural tissue and migrate toward the lesion site [34], providing a source of cells for replenishing lost neural cells. Seven days after SCI, the immunofluorescence staining results showed that Nestin-positive cells had migrated to the lesion center in all the injured mice. However, in the SCI + C-EVs and SCI + T-EVs groups, the proportion of NSCs around the epicenter was markedly greater than that in the SCI group, which indicated that MSC-released EVs can facilitate the migration of eNSCs

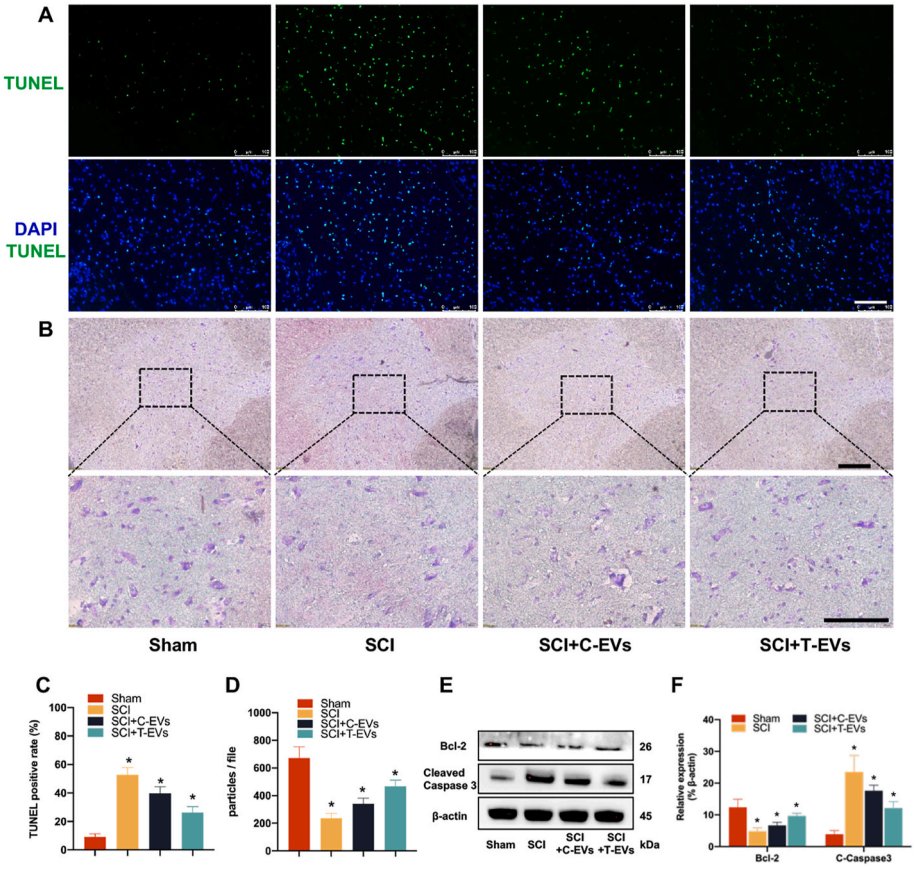

Fig. 3. T-EVs improve neuroprotection in mice subjected to SCI
(A) TUNEL staining of apoptotic cells at the injured epicenter; scale bar = 100 μm. (B) Nissl staining of residual neurons 5 mm rostral to the injured epicenter; scale bar = 100 μm. (C) Quantitative analysis of TUNEL-stained cells in the different groups. (D) Comparison of the number of Nissl bodies in the different groups. (E) Western blotting of Bcl-2, cleaved caspase-3 and β-actin in the various groups. (F) Quantification of the protein expression of Bcl-2 and cleaved caspase 3 in the different groups. *$P < 0.05$.

after SCI. Interestingly, the percentage of Nestin-positive cells around the lesion site was significantly greater in T-EV-treated SCI mice than in C-EV-treated SCI mice, suggesting that T-EVs enhance the activation of eNSCs in SCI (Fig. 4A–B). Similarly, the Western blot results demonstrated that the expression of NSC markers (Nestin and SOX2) in the SCI + T-EVs group was greater than that in the SCI + C-EVs and SCI groups (Fig. 4C–D). Previous studies have confirmed the vital role of the mTORC2/Rictor pathway in regulating cell migration, cytoskeletal rearrangement, survival and proliferation [35], and Western blotting also revealed that the mTORC2/Rictor pathway was upregulated after the application of T-EVs following SCI (Fig. 4E–F).

2.6. T-EVs facilitate neurite outgrowth and reduce glial scarring in SCI mice

In addition to the increased activation of endogenous NSCs, neurite outgrowth was also improved. The size of the SCI lesion was evaluated using HE staining at 8 weeks postsurgery. In comparison to those in the SCI group, the sagittal sections of the spinal cord tissue in both the SCI + T-EVs and SCI + C-EVs groups exhibited significantly reduced cavity areas. (Fig. 5A). Furthermore, the immunofluorescence staining images showed that the proportions of cells expressing the neurofilament outgrowth marker NF-200 in the SCI + T-EVs group were greater than those in the other SCI groups and were reduced stepwise in the SCI + C-EVs and control groups. GFAP expression was highest in the control group, followed by the SCI + C-EVs and SCI + T-EVs groups (Fig. 5B–E). The Western blot results for NF-200 and GFAP were consistent with the immunofluorescence staining findings. Treatment with T-EVs resulted in increased expression of NF-200 and decreased expression of the astrocyte marker GFAP. (Fig. 5F and G).

2.7. T-EVs enhance axonal regrowth and remyelination in SCI mice

Axonal regeneration is a crucial aspect of SCI treatment. Luxol fast

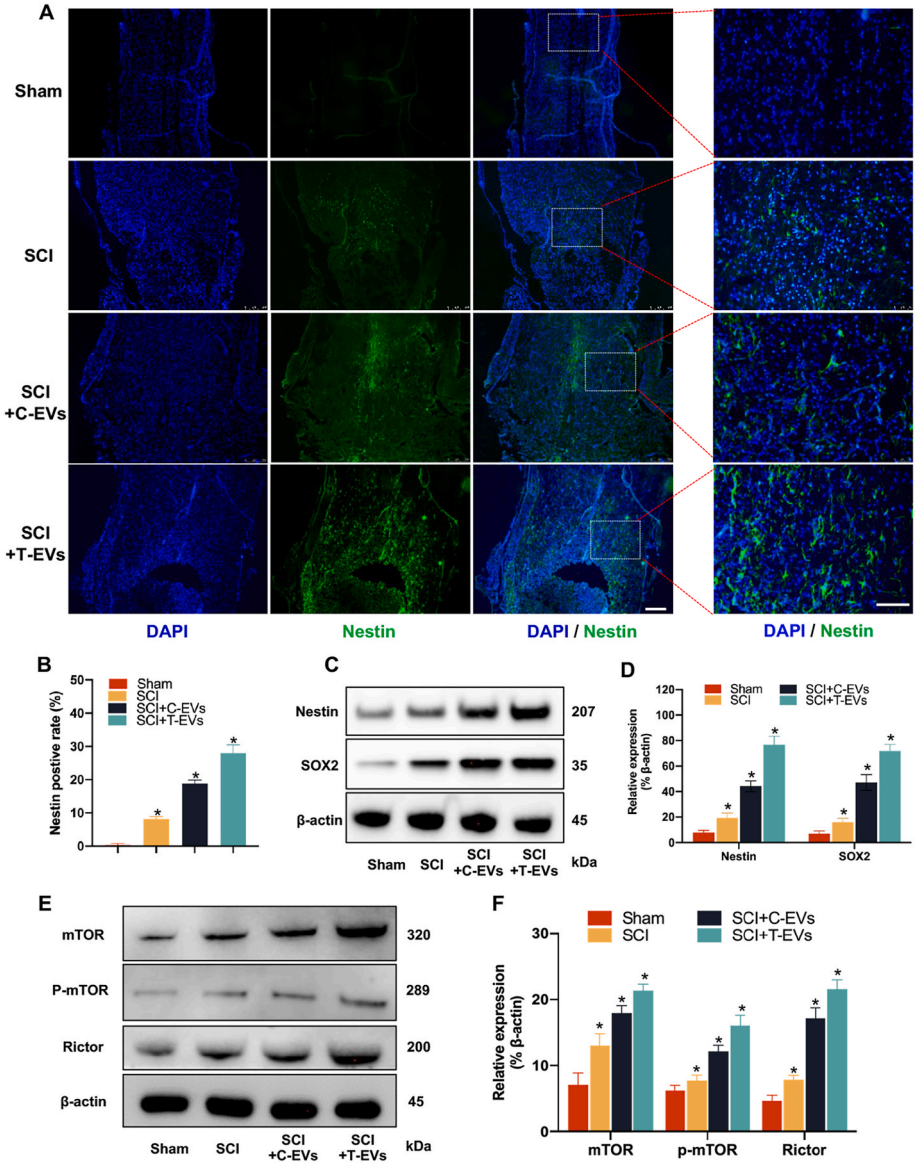

Fig. 4. T-EVs increase eNSCs around the epicenter and upregulate the mTORC2/Rictor pathway in mice with SCI
(A) Immunofluorescence staining of NSCs (Nestin^{+}) around the lesion site in the different groups; low magnification: scale bar = 250 μm; high magnification: scale bar = 50 μm. (B) Quantitative analysis of cells stained with Nestin in different groups. (C) Western blotting of NSC markers (Nestin and SOX2) and β-actin in the various groups. (D) Quantification of the protein expression of Nestin and SOX2 in the different groups. (E) Western blotting of mTORC2/Rictor pathway-related proteins and β-actin in the various groups. (F) Quantification of pmTORC2/Rictor pathway-related proteins in the different groups. *$P < 0.05$.

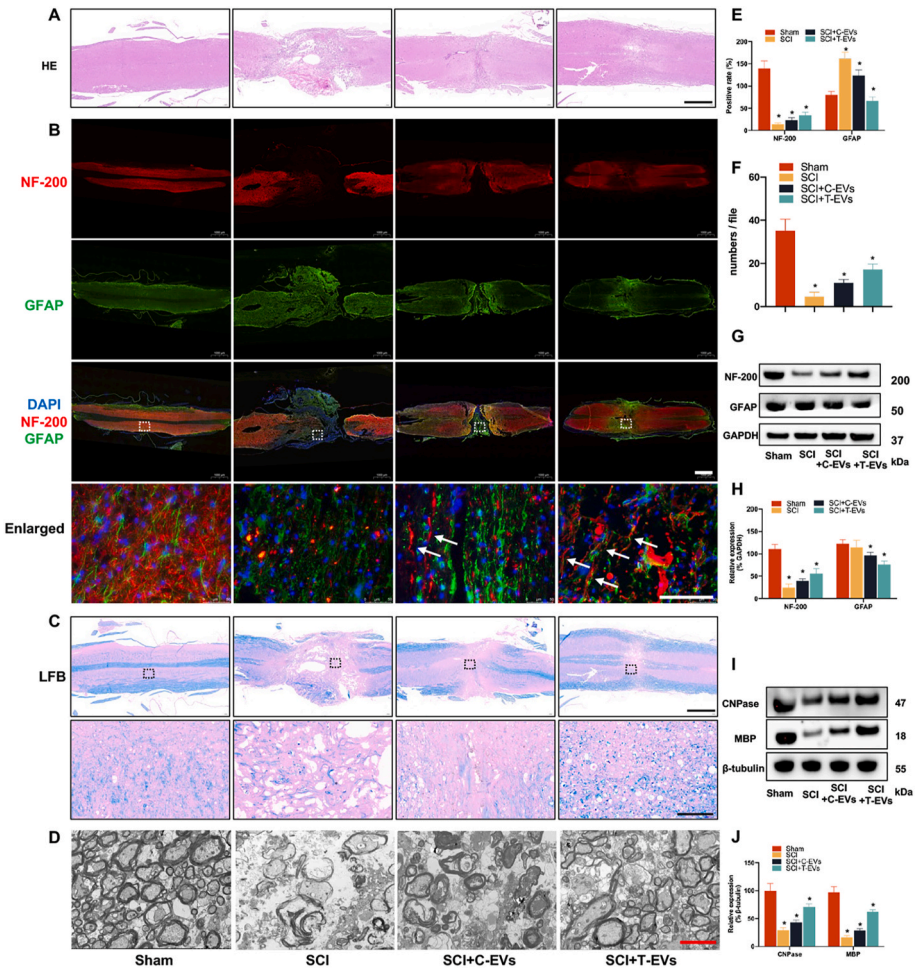

Fig. 5. T-EVs facilitate neurite outgrowth, reduce glial scarring and enhance axonal regrowth and remyelination in SCI mice
(A) HE staining of spinal cord sections from the different groups; scale bar = 1000 μm. (B) Immunofluorescence staining of NF-200 and GFAP in spinal cord sections from the different groups; low magnification: scale bar = 1000 μm; high magnification: scale bar = 100 μm. (C) LFB staining of the myelin sheath in spinal cord sections from the different groups; low magnification: scale bar = 1000 μm; high magnification: scale bar = 100 μm. (D) Electron microscopic scan of myelinated axons at the lesion site in the different groups; scale bar = 2 μm. (E) Quantitative analysis of spinal cord sections stained with NF-200 and GFAP. (F) Western blotting of NF-200, GFAP and GAPDH protein expression in the various groups. (G) Quantification of the protein expression of NF-200 and GFAP in the different groups. (H) Quantification of the number of myelinated sheaths in the different groups. (I) Western blotting of CNPase, MBP and GAPDH protein expression in the various groups. (J) Quantification of the protein expression of CNPase and MBP in the various groups. *$P < 0.05$.

blue (LFB) staining (Fig. 5C) and EM (Fig. 5D–H) revealed myelin loss in all SCI groups, but the number and percentage of regenerated and myelinated axons were significantly greater in the SCI + T-EVs group than in the SCI + C-EVs and SCI groups. The number and proportion of myelinated axons were also significantly greater in the SCI + C-EVs group than in the SCI group. In addition to assessing axon morphology, Western blotting showed that mice treated with T-EVs had markedly greater levels of CNPase and MBP than did those treated with C-EVs (Fig. 5I–J).

2.8. T-EVs promote locomotor and electrophysiological recovery in SCI mice

The application of T-EVs resulted in enhanced neurite outgrowth, axonal regrowth, and remyelination in mice with SCI. Furthermore, the neural circuit plasticity of remyelinated axons was further assessed through retrograde tracing using FG. In the sham group, nearly all neurons in the ventricles at the T8 level were labeled with FG. In contrast, a significantly lower number of FG-positive neurons was observed at the T8 level in all the SCI groups, particularly in the control group. There were significantly more FG-positive neurons in the SCI + T-EVs group than in the SCI + C-EVs group (Fig. 6A–D).

Then, locomotor recovery was compared among all groups. First, the Basso Mouse Scale (BMS) was used to evaluate the mice weekly after SCI. All the mice subjected to SCI had a score of zero on the first day after the injury, which indicated the success of the SCI model. All the injured mice achieved greater BMSs from the 1st week to the 8th week, and the mice treated with T-EVs achieved notably better BMSs than did those in the other injury groups at each evaluation from the 4th week, followed by those in the SCI + C-EVs and control groups (Fig. 6E). Next, the weight-supported stepping ability of the mice was evaluated at the 8th week after SCI. The mice without SCI could support their weight on their hindlimbs easily and walk normally. The mice in the SCI + T-EVs group could stand up and walk slowly using their hindlimbs, while the mice in the C-EV-treated group could hardly stand up or walk. However, the mice in the control group could not stand up on their hindlimbs (Fig. 6B). Furthermore, electrophysiological analysis was conducted to assess whether locomotor recovery was correlated with MEP responses. Compared with those in the sham group, the MEPs in all SCI groups were weak at 8 weeks after SCI. However, the MEPs in the T-EV-treated mice with SCI were greater than those in the SCI + C-EVs and control groups and exhibited greater expression (Fig. 6C–F). These results indicate that the application of T-EVs not only facilitates axonal regeneration but also contributes to axonal plasticity and ultimately improves the recovery of

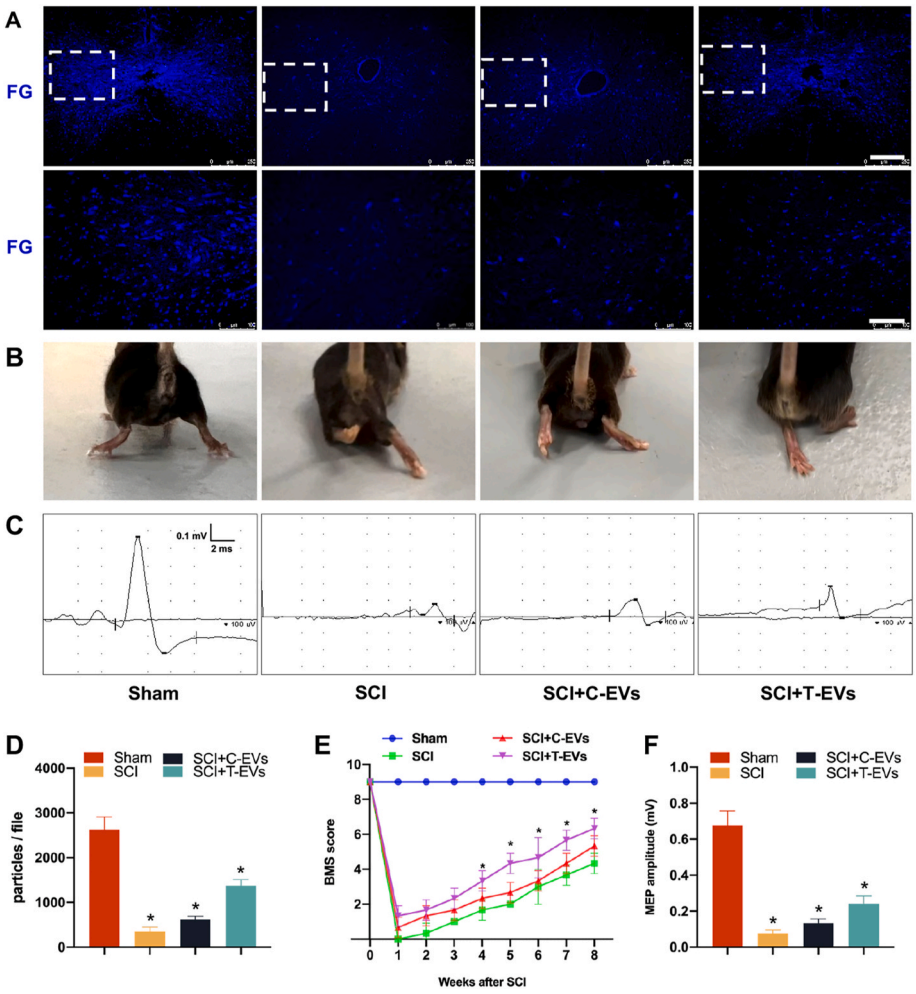

Fig. 6. T-EVs promote locomotor and electrophysiological recovery in SCI mice
(A) Fluorogold (FG)-labeled neurons in the T8 segment of the spinal cord were assessed by immunohistochemistry; scale bar = 100 μm. (B) Weight-supported stepping ability of mice in different groups at 8 weeks after SCI. (C) Representative images of MEPs in the different groups. (D) Quantification of FG-labeled neurons in the T8 segment of the spinal cord in the different groups. (E) Basso Mouse Scale (BMS) scores of mice in different groups at different time points. (F) Comparison of MEP amplitudes among groups. *$P < 0.05$.

locomotor function in rats with SCI.

2.9. T-EVs increase the activation of eNSCs and improve neurogenesis by targeting the mTORC2/Rictor pathway in mice with SCI

The aforementioned results support that the application of T-EVs increases the activation of eNSCs and subsequently enhances neurogenesis, and the mTORC2/Rictor pathway may be involved in the activation of NSCs. To further understand the correlation between T-EVs and the mTORC2/Rictor pathway in the activation of eNSCs following SCI, conditional knockout (CKO) mice in which *Rictor* was knocked out in Nestin $^{+}$ cells were used to explore the underlying mechanism. As expected, compared with those of WT mice, the number of NSCs in Rictor-deficient NSCs around the lesion site was lower after SCI. The infusion of T-EVs into *Rictor*$^{-/-}$ mice increased the number of NSCs around the SCI center compared with that in WT SCI mice. However, the ability of T-EVs to activate eNSCs following SCI in *Rictor*$^{-/-}$ mice was significantly inferior to that in WT SCI + T-EVs mice (Fig. 7A–D). Western blot analysis also revealed that, compared with that in WT SCI mice, the expression of *Nestin* in the lesion site was lower in Rictor-depleted NSCs. T-EVs dramatically increased the expression of Nestin in WT SCI + T-EVs-treated mice but slightly increased the expression of Nestin in *Rictor*$^{-/-}$ SCI + T-EVs-treated mice (Fig. 7E–F). These results indicated that T-EVs promote the activation of NSCs by enhancing the mTORC2/Rictor pathway, but other pathways may be involved. Additionally, the expression levels of P-mTOR and Rictor in the *Rictor*$^{-/-}$ SCI + T-EVs group were significantly greater than those in the *Rictor*$^{-/-}$ SCI group (Fig. 7E–F). These results suggested that T-EVs might upregulate the mTORC2/Rictor pathway in other cell types.

We further assessed whether the activation of eNSCs contributed to neuronal regeneration and functional recovery. As shown in Fig. 7B and G, compared with that in the WT SCI mice, the proportion of NF-200-positive cells in the epicenter of *Rictor*$^{-/-}$ SCI mice was markedly reduced. Similarly, the application of T-EVs to *Rictor*$^{-/-}$ mice could partly increase the percentage of NF-200-positive cells in the lesion site, but the ability of T-EVs to facilitate neurogenesis after SCI in *Rictor*$^{-/-}$ mice was significantly less than that in WT SCI mice. Interestingly, the elimination of *Rictor* in NSCs tended to result in the formation of glial scars, which were reflected as more GFAP-positive cells. The Western blot results for NF-200 and GFAP were similar to the immunofluorescence staining results (Fig. 7H–I). The electromyography results also demonstrated that the mean amplitude of MEPs was lower in the *Rictor*$^{-/-}$ SCI group than in the WT SCI group. The application of T-EVs to *Rictor*$^{-/-}$ SCI mice partly increased the amplitude of MEPs, but the mean amplitude of MEPs in the *Rictor*$^{-/-}$ SCI + T-EVs group was not as good as that in the WT SCI + T-EVs group (Fig. 7C–J). These results indicate that T-EVs increase the activation of eNSCs via the mTORC2/Rictor pathway and that the activation of NSCs contributes to the

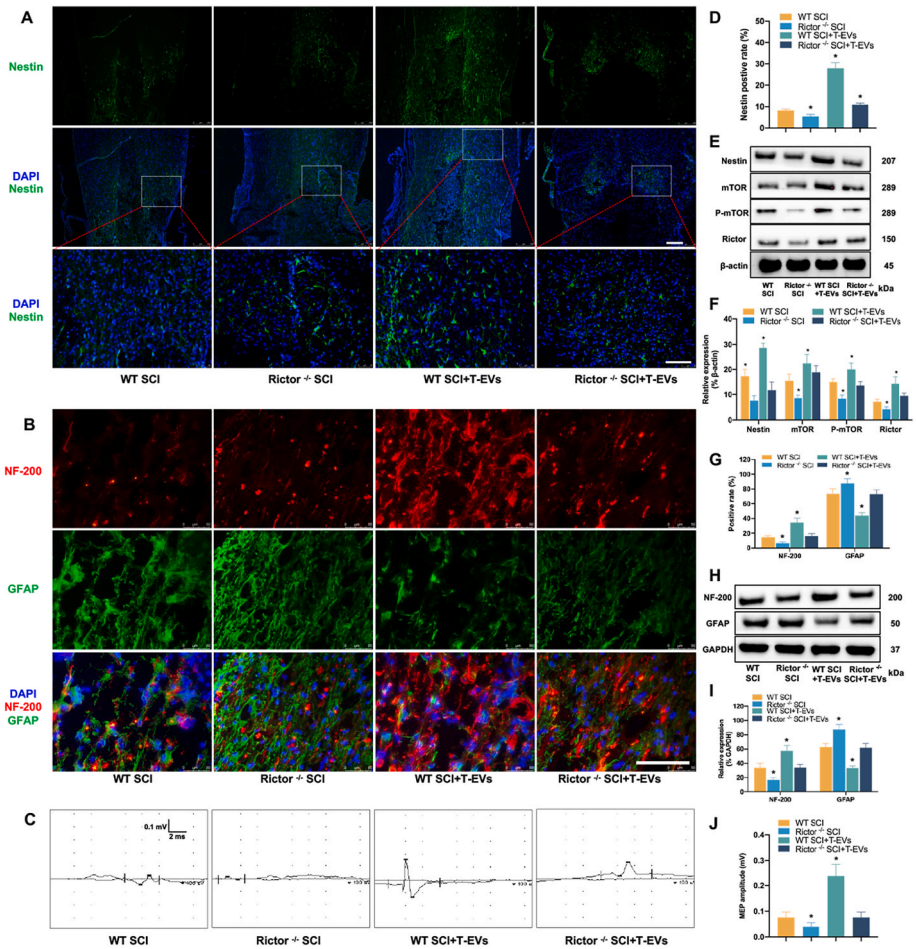

Fig. 7. T-EVs increase the activation of eNSCs and improve neurogenesis by targeting the mTORC2/Rictor pathway in mice with SCI
(A) Immunofluorescence staining of NSCs (Nestin^{+}) around the lesion site in the various groups; low magnification: scale bar = 250 μm; high magnification, scale bar = 50 μm. (B) Immunofluorescence staining of NF-200 and GFAP in spinal cord sections at 8 weeks after SCI; scale bar = 50 μm. (C) Representative images of MEPs in the different groups. (D) Percentage of cells stained with Nestin in the different groups. (E) Western blotting of Nestin, mTORC2/Rictor pathway-related proteins and β-actin in the various groups. (F) Relative expression levels of Nestin and mTORC2/Rictor pathway-related proteins in the different groups. (G) Quantitative analysis of spinal cord sections stained with NF-200 and GFAP. (H) Western blotting of NF-200, GFAP and GAPDH protein expression in the various groups. (I) Quantification of the protein expression of NF-200 and GFAP in the different groups. (J) Comparison of MEP amplitudes among groups. *$P < 0.05$.

improvement of neurogenesis and motor function.

3. Discussion

The limited production of MSC-derived EVs has been an obstacle in their application, although they have been proven to be superior at improving functional recovery after SCI [36]. In the present study, increased EV production was shown in TGF-β1-preconditioned MSCs, and the application of these EVs was first demonstrated to establish more favorable conditions for the functional restoration of SCI by reducing inflammation, attenuating residual cell apoptosis, increasing eNSC activation, promoting neuronal and axonal regeneration, and enhancing remyelination. Furthermore, the application of T-EVs in *Rictor*$^{-/-}$ SCI mice suggested that T-EVs increase the activation of eNSCs by upregulating the mTORC2/Rictor pathway.

EVs are an important component of paracrine signaling because they can mediate communication between different cells by transferring RNAs and proteins. The transplantation of EVs was proven to produce therapeutic effects and functional characteristics similar to those of cell transplantation while avoiding adverse effects [37]. The unique ability of EVs to infiltrate the blood–brain or blood–spinal cord barrier could enable them to play an important role in treating various central nervous system diseases [38]. An increasing number of studies on SCI have revealed the therapeutic potential of MSC-derived EVs for modulating neuroinflammation by shifting M1/M2 macrophage polarization and improving functional recovery. Romanelli et al. demonstrated that MSC-based EVs directly interact with activated microglia *in vitro* and reduce the production of proinflammatory cytokines during secondary injury [39]. Lankford et al. revealed that intravenously administered MSC-derived exosomes reach the SCI center quickly and specifically target M2 macrophages, consequly alleviating inflammatory reactions [40]. Fan et al. demonstrated that the combination of electroconductive hydrogels and MSC-exosomes promoted SCI recovery via immunoregulation and enhancement of myelinated axon growth [41]. To improve therapeutic efficacy, EVs were isolated from different preconditioned MSCs, and they were shown to have improved therapeutic efficacy against SCI. Exosomes from hypoxic preconditioned MSCs were confirmed to repair the SCI by shifting the M1/M2 polarization of activated microglia [42]. CD73-modified MSC-derived EVs were demonstrated to ameliorate inflammation after SCI by reducing extracellular ATP and promoting the A2bR/cAMP/PKA pathway and M2 polarization [43]. TGF-β1 has been shown to exert tissue-specific stimulatory or inhibitory effects on a variety of cellular functions, including migration, proliferation, apoptosis and differentiation [44,45]. Moreover, TGF-β1 was confirmed to play a role in various neural cells in central nervous system diseases [46]. Machika et al. reported that

increased levels of TGF-β1 in the systemic environment promote oligodendrocyte maturation, while the administration of TGF-β1 promoted remyelination and restored neurological function in a multiple sclerosis animal model [47]. Julia et al. revealed that TGF-β1 rescues neurite outgrowth under growth-inhibitory conditions via the canonical TGFβR2/ALK5 signaling axis in an *in vitro* stroke neurite outgrowth model [48]. Park et al. demonstrated the positive physiological roles of TGF-β1 in the differentiation, migration, proliferation and antiapoptotic characteristics of cultured spinal cord-derived neural progenitor cells [49]. In this study, rather than administering TGF-β1 or MSC-based EVs directly, for the first time, EVs secreted by TGF-β1-preconditioned MSCs (T-EVs) were isolated and applied to SCI mice. Our results indicated that T-EVs had a greater ability than control EVs to promote functional recovery in mice after SCI.

Inflammation and apoptosis are the two major processes involved in secondary injury following SCI [50]. SCI-induced inflammation involves microglial activation, preponderant M1 polarization, and upregulation of proinflammatory cytokines such as TNF-α, IL-1β, and IL-6. Aggravated M1 polarization and neuroinflammation result in the death or dysfunction of residual cells, which prevents the repair of SCI. Conversely, the M2 phenotype suppresses the excessive inflammatory response and promotes neurogenesis by producing anti-inflammatory cytokines [51–53]. Accumulating evidence has revealed that therapeutic efficacy in treating SCI can be improved by shifting M1/M2 polarization and reducing proinflammatory cytokine expression [54,55]. Increasing M2 polarization of microglia could improve recovery from SCI by increasing M2 phenotype-derived anti-inflammatory cytokines and providing a relatively favorable microenvironment [56]. Additionally, M2 macrophage activation facilitates spinal cord repair in SCI, which may be associated with reducing apoptosis and promoting neuronal survival [57]. In the present study, similar to the findings of previous studies, our results demonstrated that both C-EVs and T-EVs can increase M2 macrophage polarization and the expression of anti-inflammatory cytokines, reduce proinflammatory cytokines, and improve the survival of residual neurons in the acute phase of SCI. As expected, T-EVs shift M1/M2 polarization, alleviate neuroinflammation and protect residual cells more effectively than C-EVs. Interestingly, increased eNSCs around the lesion site and upregulation of the mTORC2/Rictor pathway were observed in both EV-treated groups, especially in the T-EV-treated SCI mice.

NSCs were found to primarily exist in a quiescent state within the spinal cord and are activated to proliferate, generate progeny and migrate toward the epicenter after SCI [58,59]. Indeed, studies have proven that the activation of eNSCs correlates with brain repair and improves functional outcomes in brain injury [60]. However, the proliferative profile of eNSCs after SCI is significantly less than that after brain injury [15]. The transplantation of neural stem cells (NSCs) is considered a promising strategy for reestablishing communication between lesion sites in the spinal cord through the insertion of new neurons between the injured axons and target neurons for SCI [61]. However, the difficulties in cell production and concerns regarding graft immunogenicity and rejection limit the application of grafted NSCs [13]. Hence, regulating the activation of eNSCs and recruiting them to contribute to SCI repair represent promising therapeutic approaches due to their potential to replace lost or damaged cells and reestablish neural networks after SCI [62]. The combination of drugs, small molecules and collagen scaffolds is regarded as a potential therapeutic strategy for treating SCI that can induce eNSCs to form neurons and restore damaged functions [9,59]. Exosomes secreted from MSCs were shown to promote the activation of eNSCs, further inducing neuronal differentiation and improving neurological function recovery in SCI [63]. In the present study, TGF-β1-treated MSC-based EVs effectively promoted proliferation, increased neurotrophic factor secretion, enhanced antiapoptotic activity and improved the neuronal differentiation of NSCs *in vitro*. Similar results, including increased eNSCs around the lesion site and improved neuronal and axonal regeneration, were also observed in an *in vivo* animal SCI model. Consequently, the significantly greater BMS, rostral FG-labeled neurons and MEP amplitudes detected in T-EV-treated SCI mice suggested that the regenerated neurons and axons were able to form active neuronal relays and extend numerous axons to bridge the gap both caudally and rostrally from the injury, resulting in improved functional status of motor axonal conduction [64]. Moreover, our findings revealed that the ability of activated eNSCs to proliferate in T-EV-treated SCI mice was attributable to the upregulation of the mTORC2/Rictor pathway, and the comparative results of T-EVs in the treatment of WT and *Rictor*$^{-/-}$ SCI mice further supported the critical role of the mTORC2/Rictor pathway.

Following SCI, a series of pathological phenomena occur at the epicenter, including cell death, ischemia, excitotoxicity, edema, and immune responses, resulting in an unfavorable microenvironment that inhibits the survival and neuronal differentiation of eNSCs [58,65]. The mTORC2/Rictor signaling pathway was proven to play a vital role in mediating cell survival, proliferation and migration [66,67]. mTORC2/Rictor can promote cell survival by phosphorylating AKT and controlling AKT activity and decreasing cell apoptosis by stabilizing antiapoptotic proteins through the suppression of AKT degradation [68]. Recently, mounting evidence has revealed the role of mTORC2 in the regulation of autophagy [69], while the enhancement of autophagy has been shown to boost neural stem cell neurogenesis [70]. Consistently, the current results support the vital role of the mTORC2/Rictor signaling pathway in regulating proliferation, antiapoptosis, migration and neuronal differentiation in NSCs [71]. T-EVs enhanced the activation of NSCs via the mTORC2/Rictor pathway, further promoted the differentiation of NSCs into neurons, and facilitated tissue repair and neurological recovery in SCI. These results strongly suggested that the mTORC2/Rictor pathway is a therapeutic target for optimizing the function of eNSCs in SCI. Interestingly, in T-EV-treated *Rictor*$^{-/-}$ SCI mice, the activation and neural regeneration effects of eNSCs were inferior to those of T-EV-treated WT mice but superior to those of *Rictor*$^{-/-}$ SCI mice, suggesting that T-EVs might also regulate the fate of eNSCs via other mechanisms.

Collectively, our findings support the more favorable therapeutic effect of TGF-β1-treated MSC-based EVs in promoting recovery after SCI by increasing M2 macrophage polarization and eNSC activation and promoting neuronal and axonal regeneration and reducing neuroinflammation and cell apoptosis. The increased eNSC activation in T-EV-treated SCI mice was involved in hyperactivation of the mTORC/Rictor pathway. However, further investigations are needed to explore the molecular mechanisms of T-EVs and the effects of other factors on improving recovery after SCI. However, the detailed mechanism, including the difference between C-EVs and T-EVs, should be identified to explain why T-EVs have superior efficacy in SCI repair.

4. Conclusion

The application of TGF-β1 could be utilized to alter MSC-derived EV production. The infusion of TGF-β1-pretreated MSC-derived EVs might be a promising therapeutic approach for treating SCI. T-EVs might optimize therapeutic efficacy by enhancing the activation of eNSCs via the mTORC2/Rictor pathway.

5. Materials and methods

5.1. Ethics statement

The ethical review board of The Seventh Affiliated Hospital, Sun Yat-sen University, granted approval for all procedures under the code 2019SYSUSHDW-013.

5.2. Reagents

Detailed information regarding the reagents utilized in this study is

provided in Supplementary Tables 1 and 2 of the Supplementary file.

5.3. Animals

C57BL/6J mice, both wild type (WT) and NSC-*Rictor*$^{-/-}$, were acquired from Gempharmatech Co., Ltd., Foshan, China. The deletion of *Rictor* in these mice was achieved through the Cre–loxP recombination method. Female mice aged 8 weeks and weighing between 17 and 22 g were used in the SCI experiments. These animals were housed in a pathogen-free environment under a 12-h light/dark cycle and standard feeding practices in our laboratory's animal care facility.

5.4. Primary culture of MSCs and expansion in vitro

With parental consent and ethical committee approval, human umbilical cords were collected for this study. To ensure the homogeneity of the extracted cells from multiple donors, the umbilical cord must match the following criteria: primipara aged 25–30 years old, no obstetric complications, partus matured (38–40 weeks). MSCs were extracted from Wharton's jelly section of the umbilical cord following the adherent culture technique. Initially, the MSCs were cultured in Prim® human MSC SF-M medium enriched with 1 % primocin, marking the primary passage (P0) [72]. After reaching approximately 80 % confluence, the cells were detached using 0.25 % trypsin-EDTA and incubated at 37 °C for 4 min. For further expansion, the cells were seeded at a density of 5000 cells/cm2 in 175 cm^2 T-flasks containing 30 mL of Dulbecco's modified Eagle medium/nutrient mixture F-12 (DMEM/F12) supplemented with 2 mM L-glutamine, 10 % fetal bovine serum (FBS), and 1 % penicillin–streptomycin. The cells were cultured in a humidified incubator at 37 °C with 5 % CO_2. MSCs from the third to fourth passages were used for subsequent experimental procedures.

5.5. Flow cytometry analysis and trilineage differentiation for MSC identification

After flow cytometry and multilineage differentiation analysis for MSC characterization to analyze MSC surface markers via flow cytometry, the cells were separated into single-cell suspensions by incubating them with 0.25 % trypsin-EDTA for 4 min at 37 °C. For staining, the cells were mixed in 100 μL of cell staining buffer. To prevent nonspecific binding, the cells were incubated with phycoerythrin-labeled antibodies targeting CD19 and CD105; allophycocyanin-labeled antibodies against CD34, CD45, and CD90; and fluorescein isothiocyanate-labeled antibodies against CD73 and HLA-DR [73]. For each sample, 3 μL of the appropriate antibodies was added, and the samples were stained for 20 min on ice. After staining, the cells were washed, resuspended in cell staining buffer, and adjusted to a concentration of 1×10^6 cells/mL. A Beckman CytoFlex device (CytoFLEX LX, Beckman Coulter, Indianapolis, USA) was used for flow cytometry, and the data were interpreted with CytExpert 2.3 software (Beckman Coulter, USA).

To initiate osteogenic and adipogenic differentiation, MSCs were seeded at 5000 cells/cm^2 in 6-well plates using 2 mL of DMEM/F12 supplemented with 10 % FBS, 1 % glutamine, and 1 % penicillin–streptomycin under a humidified atmosphere of 5 % CO_2 and 37 °C. Once the MSCs reached 80 % confluence, the medium was replaced with osteogenic/adipogenic induction medium, and the medium was changed daily. Differentiation was confirmed after three weeks using Alizarin Red S and Oil Red O staining. For chondrogenic differentiation, MSCs were condensed into pellets at a density of 500,000 cells/pellet and grown in tubes with 2 mL of chondrogenic induction medium or the previously mentioned DMEM/F12 as a control in a 5 % CO_2, 37 °C environment. The medium was changed every two days. After three weeks, differentiation was assessed by performing Alcian blue staining on frozen pellet sections.

5.6. EV isolation and characterization

Untreated MSCs were cultured in DMEM/F12 enriched with 2 mM L-glutamine, 10 % FBS, and 1 % penicillin–streptomycin. In contrast, MSCs exposed to TGF-β1 were cultured in the same medium supplemented with 10 ng/ml TGF-β1. We seeded 1×10^6 MSCs in a T-300 flask and allowed them to reach 80 % confluence. The cells were then rinsed twice with PBS, after which a fresh mixture of DMEM/F12, 2 mM L-glutamine, and 1 % penicillin–streptomycin was added. After 48 h of incubation, the supernatants were collected for EV extraction.

EVs were separated from these supernatants through a series of differential centrifugation steps (300×*g* for 10 min, 2000×*g* for 10 min, 10,000×*g* for 30 min, and 100,000×*g* for 70 min), followed by a PBS wash (100,000×*g* for 70 min). All centrifugation processes were conducted at 4 °C. The isolated EVs were then suspended in PBS and stored at −80 °C.

For morphological assessment, EVs were examined via transmission electron microscopy (TEM). A 10 μl EV sample was placed on Formvar/carbon-coated grids and left at 25 °C for 10 min. After removing the surplus fluid, the EVs were negatively stained with 3 % aqueous phosphotungstic acid for 5 min. Observations were made with a HITACHI HT7700 transmission electron microscope at 80 kV. Additionally, the presence of EV markers was confirmed by Western blot analysis. The size and concentration of the EVs were determined using Nano-Flow cytometry based on the NanoAnalyzer (Nanofcm, Xiamen, China).

5.7. NSC isolation and culture

NSCs were harvested from the spinal cords of 14 newborn WT C57BL/6J and *Rictor*$^{-/-}$ C57BL/6J mice following the protocol outlined in our previous study, with some modifications [74]. The procedure involved finely dissecting spinal cord tissue and dissociating it in Hanks' balanced salt solution under a microscope. This was followed by filtering the solution through 40 μm mesh filters twice. The resultant cell suspension was then spun at 1000 rpm for 5 min. The supernatant was removed, leaving behind a pellet, which was subsequently reconstituted into a single-cell suspension. For cultivation, NSCs were placed in 25 cm^2 T-flasks using growth medium composed of DMEM/F12, 2 % B-27 supplement, 1 % penicillin/streptomycin, 1 % L-glutamine, 20 ng/mL fibroblast growth factor-2 (FGF-2), and 20 ng/mL epidermal growth factor (EGF). These cells were maintained at 37 °C in a 5 % CO_2 atmosphere. The neurospheres were passaged using Accutase once they reached a diameter of approximately 100 μm. The NSCs utilized in this study were between passages 2 and 3.

5.8. Proliferation assay

NSCs were prepared as single-cell suspensions and seeded into 12-well plates at a concentration of 5×10^4 cells/well. The same expansion medium as mentioned earlier was used, with the addition of 10 μg/mL EVs. After 48 h, 20 μM 5-ethynyl-2′-deoxyuridine (EdU) was added to the culture medium. Following a further 24-h incubation, the cells were fixed with 4 % paraformaldehyde (PFA) for 30 min. The sections were then treated with Apollo® reaction cocktails for 30 min at room temperature and counterstained with Prolong Gold Antifade Reagent containing 4′-6-diamidino-2-phenylindole (DAPI) according to the instructions of the Cell-Light EdU DNA Cell Proliferation Kit.

5.9. Inducing the neuronal differentiation of NSCs

Neurospheres were separated into single-cell suspensions and seeded onto 0.01 % poly-L-lysine-coated coverslips. The seeding densities were 5×10^4 cells per well in 12-well plates and 1×10^6 cells per well in 6-well plates. Initially, the cells were cultured in expansion medium for 24 h for postpassage recovery. Subsequently, the medium was replaced with fresh differentiation medium comprising neurobasal medium, 2 %

B-27 supplement, 1 % penicillin/streptomycin, and 1 % L-glutamine. Ten micrograms of EVs were also added to the media. This differentiation medium was refreshed every two days. Fourteen days after initiating differentiation, the cells were collected for immunofluorescence staining and Western blot analysis.

5.10. Surgical procedures and EV infusion

Contusive SCI was performed using a New York University impactor as described previously [5,75]. Mice were allowed to adapt for one week, anesthetized with 5 % isoflurane for 3–4 min, and then maintained under 2.5 % isoflurane during surgery. The stabilization of the spine was achieved by clamping the transverse processes of T11 and T12. A 10-g rod was dropped from a height of 6.25 mm onto the exposed dorsal surface of the spinal cord to create the injury. Postinjury, the muscle and skin layers were sutured, and 100 μL of PBS or 200 μg/100 μL EV was administered intravenously via the tail vein [76] and at weekly intervals thereafter until the time of sacrifice. Postoperative care involved placing the mice in a controlled temperature and humidity environment, with thrice-daily manual bladder emptying until reflex bladder function was restored.

5.11. EV distribution in SCI mice

The filtered CM was incubated with 1 mM fluorescent lipophilic tracer DiR (1,1-dioctadecyl-3,3,3,3-tetramethylindotricarbocyanine iodide) (D12731; Invitrogen, Life Technologies) at room temperature for 15 min prior to EV isolation by centrifugation, as described above. To analyze the distribution of EVs in SCI mice, an IVIS Spectrum (Lumina Series III) was used. The IVIS is an instrument that contains a high-sensitivity CCD camera that enables both fluorescence and luminescence measurements. Here, live (isoflurane-sedated) mice were imaged. The live mice or the harvested organs were imaged for 1–2 s (excitation 710 nm, emission 760 nm). The data were analyzed with IVIS software (Living Image Software for IVIS).

5.12. Functional evaluation (BMS)

The BMS is based on a scale of 0 (completely paralyzed) to 9 (completely normal). The mice were placed on a plane and observed for 5 min, and hind limb motor function was scored by two independent observers blinded to the groups using a single-blind method. The average BMS of the two observers for the two hind limbs was used for analysis.

5.13. Axonal tracing

In the 7th week after surgery, a subset of mice was chosen for retrograde axonal tracing. Neuronal cell bodies projecting to the spinal segments below the graft site were marked with fluorogold (FG). Dorsal laminectomy at the T12 level was performed, followed by the injection of 0.5 μl of FG into the spinal cord using a Hamilton syringe. One week after the injection, the mice were euthanized. The T8 spinal cord segment was then harvested, cryoprotected in graded sucrose solutions, and sectioned into 10-μm thick slices [74]. These sections were examined under a confocal laser scanning microscope (Model 880, Carl Zeiss AG, Germany) to identify and count FG-positive neurons in the ventral columns. Two independent evaluators, blinded to the treatment of the rats, quantified the number of FG-labeled axons. Mice subjected to FG injection were excluded from locomotor function assessments.

5.14. MEP recording

Eight weeks after SCI, the MEPs of the various groups were recorded. The mice were anesthetized and stereotactically positioned until the T5-L1 vertebrae were completely exposed. The stimulation electrode was inserted into the T5-T6 interspinous ligaments, and a pair of needle electrodes was inserted into the interspinous ligaments of T12-L1 for MEP recording. A standardized stimulus of 0.5 mA, lasting 0.5 ms, with a 2-ms interstimulus interval and frequency of 1 Hz was administered. The amplitude of the MEP was determined from the onset to the peak of the first response wave. The peak-to-peak (P–P) amplitude was calculated to assess nerve conduction in the hindlimbs.

5.15. Tissue processing

Eight weeks after SCI, tissues were extracted from the mice. Following anesthesia, the rats underwent transcardial perfusion with 0.9 % normal saline. A 1-cm segment of the spinal cord encompassing the lesion site was then excised for Western blot analysis. Additionally, the other mice were further perfused with phosphate-buffered saline (PBS, pH 7.4) and 4 % paraformaldehyde (PFA). These spinal cord segments were similarly extracted, postfixed overnight in 4 % PFA, and then immersed in 10 % and subsequently 30 % sucrose solutions until the tissue sank. The tissue samples were embedded in optimal cutting temperature compound, frozen at −20 °C, and sectioned into 10 μm slices using a cryostat (Thermo Fisher Scientific, Waltham, MA).

5.16. Immunofluorescence (IF) staining

For IF staining, coverslips containing either cells or spinal cord tissue sections were initially fixed in 4 % PFA for 30 min. The sections were then permeabilized and blocked using a mixture of 0.3 % Triton X-100 and 5 % bovine serum albumin (BSA) for 1 h. The samples were incubated overnight at 4 °C with primary antibodies targeting specific antigens. After washing with PBS three times, the sections were treated with the appropriate secondary antibodies for 1 h at room temperature. After antibody treatment, the samples were washed three times in PBS and mounted using Prolong Gold Antifade Reagent, which included DAPI for nuclear staining. Using a confocal laser scanning microscope, the number of cells expressing the targeted markers was quantified in each visual field. Five random fields in each tissue section from each group (n = 5 per group) were examined. The antibodies utilized in the study were diluted according to the manufacturer's guidelines, and the specific details are provided in Table 2.

5.17. Western blot

Cellular lysates were extracted from cells cultured in 6-well plates and from SCI tissue. The cells and tissues were lysed in RIPA buffer to extract total protein. Subsequently, the protein concentration was determined using a BCA protein quantitation kit and standardized prior to loading. The samples were then subjected to SDS–PAGE (10 % Bis–Tris Gel), followed by transfer to polyvinylidene fluoride membranes. These membranes were subsequently blocked using 5 % nonfat dry milk in TBST (50 mM Tris, 150 mM NaCl, 0.1 % Tween 20, pH 7.6) for 1 h at room temperature. This was followed by overnight incubation with primary antibodies at 4 °C. After three washes in TBST, the PVDF membranes were incubated with peroxidase-conjugated secondary antibodies for 1 h at room temperature, followed by another three washes in TBST. Immunolabeling was detected using an enhanced chemiluminescence system (Millipore, USA). Proteins from each group (n = 5 per group) were examined. All the antibodies used in this study were appropriately diluted according to the manufacturer's instructions, and the details are provided in Table 2.

5.18. RNA extraction and real-time polymerase chain reaction (RT–PCR)

The mRNA expression levels were assessed using RT–PCR as previously described. Total RNA was extracted from cells utilizing TRIzol reagent following the manufacturer's protocol. cDNA was subsequently synthesized with a reverse transcription system (Promega, Madison, WI,

USA). RT−PCR was conducted using SYBR Green PCR Master Mix on an ABI 7900 PCR detection system. The GAPDH gene served as an internal control for normalizing gene expression levels. The relative expression of the target mRNAs was determined using the ΔΔCt method. The RT−PCR primer sequences utilized in this study were obtained from Sangon Biotech (Shanghai, China) and are listed in Table 3.

5.19. Myelination observation

To evaluate myelination, the mice were anesthetized 8 weeks post-SCI and perfused with 2.5 % glutaraldehyde (25 % glutaraldehyde: 4 % PFA = 1:9). The harvested tissues were postfixed in 2.5 % glutaraldehyde, dehydrated in 1 % osmium tetroxide, dehydrated and cleared in propylene oxide. For electron microscopy (EM) observation, 50-nm ultrathin sections were double-stained with 2 % uranyl acetate and lead citrate for subsequent EM analysis.

5.20. Nissl staining

Nissl staining was performed on transverse sections rostral to the epicenter using 0.1 % cresyl violet for 20 min at 37 °C. Following rinsing in distilled water, the stained sections were differentiated in 95 % ethyl alcohol. These sections were subsequently dehydrated in increasing concentrations of ethyl alcohol and cleared in xylene. Imaging and quantification of these sections were conducted under an optical microscope (BX53, Olympus, Japan).

5.21. ELISA

Following euthanasia through cervical dislocation, the spinal cord of each mouse was promptly excised and immersed in phosphate-buffered saline (PBS). The spinal cord segment, which was precisely 1 cm in length and approximately 100 mg in weight, was then homogenized and centrifuged at 4 °C to obtain the supernatant. The concentrations of inflammatory markers, such as tumor necrosis factor-α (TNF-α), interleukin (IL)-6, IL-1β, monocyte chemotactic protein 1 (MCP-1), IL-10, and IL-4, in the spinal cord tissues were quantified using ELISA kits, strictly following the manufacturer's guidelines.

5.22. TUNEL assay

The TUNEL assay was performed utilizing a commercial kit. Tissue sections were fixed for 30 min in 4 % paraformaldehyde (PFA), followed by 15 min of permeabilization with 0.3 % Triton X-100. Subsequently, the sections were incubated with TUNEL reagent for 1 h at 37 °C in a light-protected environment. After three PBS washes, the sections were mounted with Prolong Gold Antifade Reagent containing DAPI. A confocal laser scanning microscope was used for the analysis of the stained cells.

Statistical analysis

Statistical evaluations in this study were conducted using GraphPad Prism 9 software (GraphPad Software, Inc., USA). Initially, the Shapiro–Wilk test was applied to all the data sets to confirm a normal distribution. The data are presented as the means ± standard deviations (SDs). Analytical comparisons were made using one-way ANOVA with Bonferroni post hoc correction for multiple groups or Student's *t*-test for two-group comparisons. A P value less than 0.05 indicated statistical significance.

Funding

This work was supported by the Fundamental Research Funds for the Central Universities (No. 21623310), the Dongguan Science and Technology of Social Development Program (No. 20231800939902), the National Natural Science Foundation of China (No. 81801907), the Guangdong Basic and Applied Basic Research Foundation (No. 2022A1515140171) and the Medical Joint Fund of Jinan University (No. YXJC2022011).

Ethics statement

All procedures were approved by The Seventh Affiliated Hospital of Sun Yat-sen University Ethics Committee (2019SYSUSHDW-013).

CRediT authorship contribution statement

Guoliang Chen: Writing – original draft, Funding acquisition, Conceptualization. **Shiming Li:** Investigation. **Kuileung Tong:** Investigation. **Zerong Huang:** Investigation. **Shuangjiang Liu:** Investigation. **Haoran Zhu:** Investigation. **Yanheng Zhong:** Investigation. **Zhisen Zhou:** Investigation. **Genlong Jiao:** Supervision, Project administration, Funding acquisition, Conceptualization. **Fuxin Wei:** Supervision, Project administration, Conceptualization. **Ningning Chen:** Writing – review & editing, Project administration, Funding acquisition, Conceptualization.

Declaration of competing interest

The authors declare that they have no known competing financial interests or personal relationships that could have appeared to influence the work reported in this paper.

Appendix A. Supplementary data

Supplementary data to this article can be found online at https://doi.org/10.1016/j.bioactmat.2024.01.013.

References

[1] A. Singh, L. Tetreault, S. Kalsi-Ryan, A. Nouri, M.G. Fehlings, Global prevalence and incidence of traumatic spinal cord injury, Clin. Epidemiol. 6 (2014) 309–331, https://doi.org/10.2147/CLEP.S68889.
[2] Global, regional, and national burden of traumatic brain injury and spinal cord injury, 1990-2016: a systematic analysis for the Global Burden of Disease Study 2016, Lancet Neurol. 18 (2019) 56–87, https://doi.org/10.1016/S1474-4422(18)30415-0.
[3] C.S. Ahuja, et al., Traumatic spinal cord injury-repair and regeneration, Neurosurgery 80 (2017), https://doi.org/10.1093/neuros/nyw080.
[4] A. Anjum, et al., Spinal cord injury: pathophysiology, multimolecular interactions, and underlying recovery mechanisms, Int. J. Mol. Sci. 21 (2020), https://doi.org/10.3390/ijms21207533.
[5] G. Sun, et al., γδ T cells provide the early source of IFN-γ to aggravate lesions in spinal cord injury, J. Exp. Med. 215 (2018) 521–535, https://doi.org/10.1084/jem.20170686.
[6] Y. Xu, et al., Understanding the role of tissue-specific decellularized spinal cord matrix hydrogel for neural stem/progenitor cell microenvironment reconstruction and spinal cord injury, Biomaterials 268 (2021) 120596, https://doi.org/10.1016/j.biomaterials.2020.120596.
[7] E.A.B. Gilbert, M.K. Vickaryous, Neural stem/progenitor cells are activated during tail regeneration in the leopard gecko (Eublepharis macularius), J. Comp. Neurol. 526 (2018) 285–309, https://doi.org/10.1002/cne.24335.
[8] L. McHedlishvili, et al., Reconstitution of the central and peripheral nervous system during salamander tail regeneration, Proc. Natl. Acad. Sci. U. S. A. 109 (2012) E2258–E2266, https://doi.org/10.1073/pnas.1116738109.
[9] Y. Yang, et al., Small molecules combined with collagen hydrogel direct neurogenesis and migration of neural stem cells after spinal cord injury, Biomaterials 269 (2021) 120479, https://doi.org/10.1016/j.biomaterials.2020.120479.
[10] M.A. Anderson, et al., Required growth facilitators propel axon regeneration across complete spinal cord injury, Nature 561 (2018) 396–400, https://doi.org/10.1038/s41586-018-0467-6.
[11] M. Stenudd, H. Sabelstrom, J. Frisen, Role of endogenous neural stem cells in spinal cord injury and repair, JAMA Neurol. 72 (2015) 235–237, https://doi.org/10.1001/jamaneurol.2014.2927.
[12] K. Tong, et al., Inhibition of neural stem cell necroptosis mediated by RIPK1/MLKL promotes functional recovery after SCI, Mol. Neurobiol. (2023), https://doi.org/10.1007/s12035-022-03156-z.

[13] X. Li, et al., Regenerative potential of ependymal cells for spinal cord injuries over time, EBioMedicine 13 (2016) 55–65, https://doi.org/10.1016/j.ebiom.2016.10.035.
[14] A.J. Mothe, C.H. Tator, Proliferation, migration, and differentiation of endogenous ependymal region stem/progenitor cells following minimal spinal cord injury in the adult rat, Neuroscience 131 (2005) 177–187.
[15] E.A.B. Gilbert, N. Lakshman, K.S.K. Lau, C.M. Morshead, Regulating endogenous neural stem cell activation to promote spinal cord injury repair, Cells 11 (2022), https://doi.org/10.3390/cells11050846.
[16] V.R. Dasari, K.K. Veeravalli, D.H. Dinh, Mesenchymal stem cells in the treatment of spinal cord injuries: a review, World J. Stem Cell. 6 (2014) 120–133, https://doi.org/10.4252/wjsc.v6.i2.120.
[17] W.-Z. Liu, Z.-J. Ma, J.-R. Li, X.-W. Kang, Mesenchymal stem cell-derived exosomes: therapeutic opportunities and challenges for spinal cord injury, Stem Cell Res. Ther. 12 (2021) 102, https://doi.org/10.1186/s13287-021-02153-8.
[18] Y. Lu, et al., The optimal transplantation strategy of umbilical cord mesenchymal stem cells in spinal cord injury: a systematic review and network meta-analysis based on animal studies, Stem Cell Res. Ther. 13 (2022) 441, https://doi.org/10.1186/s13287-022-03103-8.
[19] S. Reyhani, B. Abbaspanah, S.H. Mousavi, Umbilical cord-derived mesenchymal stem cells in neurodegenerative disorders: from literature to clinical practice, Regen. Med. 15 (2020) 1561–1578, https://doi.org/10.2217/rme-2019-0119.
[20] X. Yuan, et al., Cell-adaptable dynamic hydrogel reinforced with stem cells improves the functional repair of spinal cord injury by alleviating neuroinflammation, Biomaterials 279 (2021) 121190, https://doi.org/10.1016/j.biomaterials.2021.121190.
[21] K. Drela, L. Stanaszek, A. Nowakowski, Z. Kuczynska, B. Lukomska, Experimental strategies of mesenchymal stem cell propagation: adverse events and potential risk of functional changes, Stem Cell. Int. 2019 (2019) 7012692, https://doi.org/10.1155/2019/7012692.
[22] B. Chen, Q. Li, B. Zhao, Y. Wang, Stem cell-derived extracellular vesicles as a novel potential therapeutic tool for tissue repair, Stem Cells Transl Med 6 (2017) 1753–1758, https://doi.org/10.1002/sctm.16-0477.
[23] M. Nakazaki, T. Morita, K.L. Lankford, P.W. Askenase, J.D. Kocsis, Small extracellular vesicles released by infused mesenchymal stromal cells target M2 macrophages and promote TGF-β upregulation, microvascular stabilization and functional recovery in a rodent model of severe spinal cord injury, J. Extracell. Vesicles 10 (2021) e12137, https://doi.org/10.1002/jev2.12137.
[24] R. Kalluri, V.S. LeBleu, The biology function and biomedical applications of exosomes, Science 367 (2020), https://doi.org/10.1126/science.aau6977.
[25] Y. Wang, et al., Umbilical mesenchymal stem cell-derived exosomes facilitate spinal cord functional recovery through the miR-199a-3p/145-5p-mediated NGF/TrkA signaling pathway in rats, Stem Cell Res. Ther. 12 (2021) 117, https://doi.org/10.1186/s13287-021-02148-5.
[26] Y. Liang, J.-H. Wu, J.-H. Zhu, H. Yang, Exosomes secreted by hypoxia-preconditioned adipose-derived mesenchymal stem cells reduce neuronal apoptosis in rats with spinal cord injury, J. Neurotrauma 39 (2022) 701–714, https://doi.org/10.1089/neu.2021.0290.
[27] W. Liu, et al., Extracellular vesicles derived from melatonin-preconditioned mesenchymal stem cells containing USP29 repair traumatic spinal cord injury by stabilizing NRF2, J. Pineal Res. 71 (2021) e12769, https://doi.org/10.1111/jpi.12769.
[28] J. Sun, Y. Zhou, Z. Ye, W.-S. Tan, Transforming growth factor-β1 stimulates mesenchymal stem cell proliferation by altering cell cycle through FAK-Akt-mTOR pathway, Connect. Tissue Res. 60 (2019) 406–417, https://doi.org/10.1080/03008207.2019.1570171.
[29] W. Xin, et al., TGF-β1 decreases microglia-mediated neuroinflammation and lipid droplet accumulation in an in vitro stroke model, Int. J. Mol. Sci. 24 (2023), https://doi.org/10.3390/ijms242417329.
[30] C.R. Harrell, N. Jovicic, V. Djonov, N. Arsenijevic, V. Volarevic, Mesenchymal stem cell-derived exosomes and other extracellular vesicles as new remedies in the therapy of inflammatory diseases, Cells 8 (2019), https://doi.org/10.3390/cells8121605.
[31] G.Y. Liu, D.M. Sabatini, mTOR at the nexus of nutrition, growth, ageing and disease, Nat. Rev. Mol. Cell Biol. 21 (2020) 183–203, https://doi.org/10.1038/s41580-019-0199-y.
[32] G. Chen, et al., Transplanting neurofibromatosis-1 gene knockout neural stem cells improve functional recovery in rats with spinal cord injury by enhancing the mTORC2 pathway, Exp. Mol. Med. 54 (2022) 1766–1777, https://doi.org/10.1038/s12276-022-00850-9.
[33] Z. Liao, et al., Metformin facilitates mesenchymal stem cell-derived extracellular nanovesicles release and optimizes therapeutic efficacy in intervertebral disc degeneration, Biomaterials 274 (2021) 120850, https://doi.org/10.1016/j.biomaterials.2021.120850.
[34] M. Shu, et al., Single-cell RNA sequencing reveals Nestin active neural stem cells outside the central canal after spinal cord injury, Sci. China Life Sci. 65 (2022) 295–308, https://doi.org/10.1007/s11427-020-1930-0.
[35] R.A. Saxton, D.M. Sabatini, mTOR signaling in growth, metabolism, and disease, Cell 168 (2017) 960–976, https://doi.org/10.1016/j.cell.2017.02.004.
[36] C. Wang, et al., A bioactive injectable self-healing anti-inflammatory hydrogel with ultralong extracellular vesicles release synergistically enhances motor functional recovery of spinal cord injury, Bioact. Mater. 6 (2021) 2523–2534, https://doi.org/10.1016/j.bioactmat.2021.01.029.
[37] S.F. Mause, C. Weber, Microparticles: protagonists of a novel communication network for intercellular information exchange, Circ. Res. 107 (2010) 1047–1057, https://doi.org/10.1161/CIRCRESAHA.110.226456.
[38] J. Ruan, X. Miao, D. Schlüter, L. Lin, X. Wang, Extracellular vesicles in neuroinflammation: pathogenesis, diagnosis, and therapy, Mol. Ther. 29 (2021) 1946–1957, https://doi.org/10.1016/j.ymthe.2021.04.020.
[39] P. Romanelli, et al., Extracellular vesicles can deliver anti-inflammatory and anti-scarring activities of mesenchymal stromal cells after spinal cord injury, Front. Neurol. 10 (2019) 1225, https://doi.org/10.3389/fneur.2019.01225.
[40] K.L. Lankford, et al., Intravenously delivered mesenchymal stem cell-derived exosomes target M2-type macrophages in the injured spinal cord, PLoS One 13 (2018) e0190358, https://doi.org/10.1371/journal.pone.0190358.
[41] L. Fan, et al., Exosomes-loaded electroconductive hydrogel synergistically promotes tissue repair after spinal cord injury via immunoregulation and enhancement of myelinated axon growth, Adv. Sci. 9 (2022) e2105586, https://doi.org/10.1002/advs.202105586.
[42] W. Liu, et al., Exosome-shuttled miR-216a-5p from hypoxic preconditioned mesenchymal stem cells repair traumatic spinal cord injury by shifting microglial M1/M2 polarization, J. Neuroinflammation 17 (2020) 47, https://doi.org/10.1186/s12974-020-1726-7.
[43] X. Zhai, et al., Extracellular vesicles derived from CD73 modified human umbilical cord mesenchymal stem cells ameliorate inflammation after spinal cord injury, J. Nanobiotechnol. 19 (2021) 274, https://doi.org/10.1186/s12951-021-01022-z.
[44] K.D. Suson, A.A. Stec, J.P. Gearhart, L.A. Shimoda, Transforming growth factor-β1 mediates migration in cultured human control and exstrophy bladder smooth muscle cells, J. Urol. 188 (2012) 1528–1533, https://doi.org/10.1016/j.juro.2012.02.038.
[45] A.K. Kudva, A.D. Dikina, F.P. Luyten, E. Alsberg, J. Patterson, Gelatin microspheres releasing transforming growth factor drive in vitro chondrogenesis of human periosteum derived cells in micromass culture, Acta Biomater. 90 (2019) 287–299, https://doi.org/10.1016/j.actbio.2019.03.039.
[46] S. Li, X. Gu, S. Yi, The regulatory effects of transforming growth factor-β on nerve regeneration, Cell Transplant. 26 (2017) 381–394, https://doi.org/10.3727/096368916X693824.
[47] M. Hamaguchi, et al., Circulating transforming growth factor-β1 facilitates remyelination in the adult central nervous system, Elife 8 (2019), https://doi.org/10.7554/eLife.41869.
[48] J. Kaiser, et al., TGFβ1 induces axonal outgrowth via ALK5/PKA/SMURF1-Mediated degradation of RhoA and stabilization of PAR6, eNeuro 7 (2020), https://doi.org/10.1523/ENEURO.0104-20.2020.
[49] S.M. Park, J.S. Jung, M.S. Jang, K.S. Kang, S.K. Kang, Transforming growth factor-beta 1 regulates the fate of cultured spinal cord-derived neural progenitor cells, Cell Prolif. 41 (2008) 248–264, https://doi.org/10.1111/j.1365-2184.2008.00514.x.
[50] Y. Rong, et al., Neural stem cell-derived small extracellular vesicles attenuate apoptosis and neuroinflammation after traumatic spinal cord injury by activating autophagy, Cell Death Dis. 10 (2019) 340, https://doi.org/10.1038/s41419-019-1571-8.
[51] J. Lin, et al., Neuroprotective effect of ketone metabolism on inhibiting inflammatory response by regulating macrophage polarization after acute cervical spinal cord injury in rats, Front. Neurosci. 14 (2020) 583611, https://doi.org/10.3389/fnins.2020.583611.
[52] H. Fan, et al., Reactive astrocytes undergo M1 microglia/macrohpages-induced necroptosis in spinal cord injury, Mol. Neurodegener. 11 (2016) 14, https://doi.org/10.1186/s13024-016-0081-8.
[53] X. Liu, et al., Salidroside provides neuroprotection by modulating microglial polarization after cerebral ischemia, J. Neuroinflammation 15 (2018) 39, https://doi.org/10.1186/s12974-018-1081-0.
[54] K. Shen, et al., Anti-inflammatory nanotherapeutics by targeting matrix metalloproteinases for immunotherapy of spinal cord injury, Small 17 (2021) e2102102, https://doi.org/10.1002/smll.202102102.
[55] P. Peng, et al., Exosomes-mediated phenotypic switch of macrophages in the immune microenvironment after spinal cord injury, Biomedicine & Pharmacotherapy = Biomedecine & Pharmacotherapie 144 (2021) 112311, https://doi.org/10.1016/j.biopha.2021.112311.
[56] N. Chen, et al., Overexpression of Rictor in the injured spinal cord promotes functional recovery in a rat model of spinal cord injury, Faseb. J. 34 (2020) 6984–6998, https://doi.org/10.1096/fj.201903171R.
[57] J. Park, et al., Local immunomodulation with anti-inflammatory cytokine-encoding lentivirus enhances functional recovery after spinal cord injury, Mol. Ther. 26 (2018) 1756–1770, https://doi.org/10.1016/j.ymthe.2018.04.022.
[58] X. Li, et al., Scaffold-facilitated locomotor improvement post complete spinal cord injury: motor axon regeneration versus endogenous neuronal relay formation, Biomaterials 197 (2019) 20–31, https://doi.org/10.1016/j.biomaterials.2019.01.012.
[59] X. Li, et al., Cetuximab modified collagen scaffold directs neurogenesis of injury-activated endogenous neural stem cells for acute spinal cord injury repair, Biomaterials 137 (2017) 73–86, https://doi.org/10.1016/j.biomaterials.2017.05.027.
[60] P. Dadwal, et al., Activating endogenous neural precursor cells using metformin leads to neural repair and functional recovery in a model of childhood brain injury, Stem Cell Rep. 5 (2015) 166–173, https://doi.org/10.1016/j.stemcr.2015.06.011.
[61] W. Xue, et al., Direct neuronal differentiation of neural stem cells for spinal cord injury repair, Stem Cell. 39 (2021) 1025–1032, https://doi.org/10.1002/stem.3366.
[62] E. Llorens-Bobadilla, et al., A latent lineage potential in resident neural stem cells enables spinal cord repair, Science 370 (2020), https://doi.org/10.1126/science.abb8795.

[63] W. Zhou, et al., Exosomes derived from human placental mesenchymal stem cells enhanced the recovery of spinal cord injury by activating endogenous neurogenesis, Stem Cell Res. Ther. 12 (2021) 174, https://doi.org/10.1186/s13287-021-02248-2.
[64] P. Lu, et al., Long-distance growth and connectivity of neural stem cells after severe spinal cord injury, Cell 150 (2012) 1264–1273, https://doi.org/10.1016/j.cell.2012.08.020.
[65] T. Hagg, M. Oudega, Degenerative and spontaneous regenerative processes after spinal cord injury, J. Neurotrauma 23 (2006) 264–280.
[66] S.D. Wahane, et al., PI3K-p110-alpha-subtype signalling mediates survival, proliferation and neurogenesis of cortical progenitor cells via activation of mTORC2, J. Neurochem. 130 (2014) 255–267, https://doi.org/10.1111/jnc.12718.
[67] H. Senoo, et al., Phosphorylated Rho-GDP directly activates mTORC2 kinase towards AKT through dimerization with Ras-GTP to regulate cell migration, Nat. Cell Biol. 21 (2019) 867–878, https://doi.org/10.1038/s41556-019-0348-8.
[68] W.J. Oh, E. Jacinto, mTOR complex 2 signaling and functions, Cell Cycle 10 (2011) 2305–2316.
[69] J. Ballesteros-Álvarez, J.K. Andersen, mTORC2: the other mTOR in autophagy regulation, Aging Cell 20 (2021) e13431, https://doi.org/10.1111/acel.13431.
[70] L. He, et al., Electrical stimulation at nanoscale topography boosts neural stem cell neurogenesis through the enhancement of autophagy signaling, Biomaterials 268 (2021) 120585, https://doi.org/10.1016/j.biomaterials.2020.120585.
[71] G. Chen, et al., Transplanting neurofibromatosis-1 gene knockout neural stem cells improve functional recovery in rats with spinal cord injury by enhancing the mTORC2 pathway, Exp. Mol. Med. (2022), https://doi.org/10.1038/s12276-022-00850-9.
[72] P. Guo, et al., A single-cell transcriptome of mesenchymal stromal cells to fabricate bioactive hydroxyapatite materials for bone regeneration, Bioact. Mater. 9 (2022) 281–298, https://doi.org/10.1016/j.bioactmat.2021.08.009.
[73] P. Zhang, et al., Effect of cyclic mechanical loading on immunoinflammatory microenvironment in biofabricating hydroxyapatite scaffold for bone regeneration, Bioact. Mater. 6 (2021) 3097–3108, https://doi.org/10.1016/j.bioactmat.2021.02.024.
[74] N. Chen, et al., Targeted inhibition of leucine-rich repeat and immunoglobulin domain-containing protein 1 in transplanted neural stem cells promotes neuronal differentiation and functional recovery in rats subjected to spinal cord injury, Crit. Care Med. 44 (2016) e146–e157, https://doi.org/10.1097/CCM.0000000000001351.
[75] J.A. Gruner, A monitored contusion model of spinal cord injury in the rat, J. Neurotrauma 9 (1992).
[76] C. Liu, et al., Dental pulp stem cell-derived exosomes suppress M1 macrophage polarization through the ROS-MAPK-NFκB P65 signaling pathway after spinal cord injury, J. Nanobiotechnol. 20 (2022) 65, https://doi.org/10.1186/s12951-022-01273-4.